A T7 phage factor required for managing RpoS in *Escherichia coli*

Aline Tabib-Salazar[2, a], Bing Liu[1, a], Declan Barkar[2], Lynn Burchell[2], Udi Qimron[3], Steve J. Matthews[2, *] and Sivaramesh Wigneshweraraj[2, *]

[1]BioBank, First Affiliated Hospital, School of medicine, Xi'an Jiaotong University, Shaanxi Sheng, China; [2]MRC Centre for Molecular Bacteriology and Infection, Imperial College London, London, SW7 2AZ, UK; [3]Department of Clinical Microbiology and Immunology, Sackler School of Medicine, Tel Aviv University, Tel Aviv 69978, Israel.

To whom correspondence should be addressed**:** Sivaramesh Wigneshweraraj or Steve Matthews, MRC Centre for Molecular Bacteriology and Infection, Imperial College London, London, SW7 2AZ, UK. E-mail: s.r.wig@imperial.ac.uk or s.j.matthews@imperial.ac.uk

T7 development in *Escherichia coli* requires the inhibition of the housekeeping form of the bacterial RNA polymerase (RNAP), Eσ^{70}, by two T7 proteins: Gp2

and Gp5.7. While the biological role of Gp2 is well understood, that of Gp5.7 remains to be fully deciphered. Here, we present results from functional and structural analyses to reveal that Gp5.7 primarily serves to inhibit Eσ^S, the predominant form of the RNAP in the stationary phase of growth, which accumulates in exponentially growing *E. coli* as a consequence of buildup of guanosine pentaphosphate ((p)ppGpp) during T7 development. We further demonstrate a requirement of Gp5.7 for T7 development in *E. coli* cells in the stationary phase of growth. Our finding represents a paradigm for how some lytic phages have evolved distinct mechanisms to inhibit the bacterial transcription machinery to facilitate phage development in bacteria in the exponential and stationary phases of growth.

Acquisition of the bacterial transcription machinery, the RNA polymerase (RNAP), is a major mechanism by which bacteriophages reprogram cellular processes in the host

51 in order to mount a successful infection. The prototypical lytic phage of *Escherichia*
52 *coli*, T7, synthesizes three proteins, Gp0.7, Gp2 and Gp5.7, that interact with host
53 RNAP, to facilitate the temporal coordinated expression of its genome. The genes of
54 T7 are categorized as early, middle and late to reflect the timing of their expression
55 during the infection process. Early and middle genes generally encode proteins
56 required for phage RNA synthesis, DNA replication and host takeover, whereas the
57 late genes specify T7 virion assembly and structural proteins. The translocation of the
58 T7 genome into *E. coli* is a transcription-coupled process and requires the
59 housekeeping form of the host RNAP ($E\sigma^{70}$) to transcribe the early genes from three
60 strong early gene promoters, T7 A1, A2 and A3, and catalyze the entry of T7 DNA
61 into the cell [1]. The coordinated action of the early gene product Gp0.7 and the
62 essential middle gene product Gp2 subsequently shuts off $E\sigma^{70}$ activity on the T7
63 genome. The viral single-subunit RNAP (T7 RNAP, Gp1, a product of an early gene)
64 transcribes the middle and late viral genes. The shutting down of host RNAP is
65 crucial for the coordination of the activities of bacterial and phage RNAPs on the
66 phage genome and thus consequently for successful completion of the infection cycle:
67 Gp0.7 is a protein kinase that phosphorylates $E\sigma^{70}$, leading to increased transcription
68 termination at sites located between the early and middle genes on the T7 genome [2, 3];
69 Gp2 binds in the main DNA binding channel of $E\sigma^{70}$ and thereby prevents the
70 formation of the transcriptionally-proficient open promoter complex (RPo) at the T7
71 A1-3 promoters [4]. Gp2 is indispensable for T7 growth. In a T7 Δ*gp2* phage, aberrant
72 transcription of middle and late T7 genes (that are normally transcribed by the T7
73 RNAP) by $E\sigma^{70}$ results in interference between the two RNAPs and, consequently, in
74 aborted infection [2]. Recently, a T7 middle gene product, Gp5.7, was identified as a
75 repressor of RPo formation specifically on the T7 A1-3 promoters by $E\sigma^{70}$ molecules,

76 which might have escaped inhibition by Gp2[5]. However, since phage genomes tend to
77 be compact and efficient, it is puzzling that T7 has evolved two markedly different
78 proteins to inhibit Eσ^{70}, especially since Gp5.7, unlike Gp2, is a relatively poor
79 inhibitor of Eσ^{70} [5]. In this study, we unveil additional biological roles for Gp5.7
80 during T7 development in *E. coli*.
81
82 **Results**
83
84 **Gp5.7 is an inhibitor of the *E. coli* stationary phase RNAP, Eσ^S**
85 Previously, we posited that Gp5.7 prevents transcription initiation from T7 A1-A3
86 promoters by Eσ^{70} that might have escaped inhibition by Gp2 [5]. While this still
87 remains a role for Gp5.7 in T7 development in *E. coli*, we noted a report by Friesen
88 and Fill describing the accumulation of the stress signaling nucleotide guanosine
89 pentaphosphate, (p)ppGpp, in a valine auxotroph strain of *E. coli* during T7
90 development [6]. Since (p)ppGpp simultaneously induces σ^S transcription and
91 accumulation of σ^S (the predominant σ factor active in stationary phase *E. coli*) and,
92 considering that Gp5.7 is an inefficient inhibitor of Eσ^{70} compared to Gp2 [5], we
93 contemplated whether Gp5.7 might preferentially inhibit Eσ^S over Eσ^{70}. Initially, we
94 established that (p)ppGpp does indeed accumulate during T7 development in
95 exponentially growing wild-type *E. coli* cells (Figure 1a). We further demonstrated
96 that the accumulation of (p)ppGpp is accompanied by an increase in the intracellular
97 levels of σ^S during T7 development in exponentially growing *E. coli* (Figure 1b).
98 Control experiments with a *relA*/*spoT* mutant *E. coli* strain confirmed that the
99 accumulation of σ^S during T7 infection was indeed (p)ppGpp-dependent (Figure 1b).
100 Next, we established that Eσ^S could initiate transcription form the T7 A1 promoter as

101 efficiently as $E\sigma^{70}$ (Figure 1c, compare lanes 1 and 8) and that $E\sigma^{S}$ activity on the T7
102 A1 promoter is effectively inhibited by Gp5.7 (Figure 1c, lanes 12-13). Control
103 experiments with a functionally defective mutant of Gp5.7 (Gp5.7-L42A [5]) confirmed
104 that the inhibition of $E\sigma^{S}$ activity on the T7 A1 promoter by Gp5.7 was specific
105 (Supplementary Figure 1). Strikingly, it seems that Gp5.7 is a more efficient inhibitor
106 of $E\sigma^{S}$ than of $E\sigma^{70}$ (Figure 1c). In contrast and consistent with previous observations
107 [4], Gp2 is a more effective inhibitor of $E\sigma^{70}$ than $E\sigma^{S}$ (Figure 1c). Overall, we conclude
108 that Gp5.7 and Gp2 are both required to fully shutdown the $E\sigma^{70}$ and $E\sigma^{S}$ to allow
109 optimal T7 development in *E. coli* cells during the exponential phase of growth.
110
111 **Gp5.7 interacts with region 4 of σ^{S}**
112 Although Gp5.7 interacts with the core subunits of the RNAP [5], our results indicate
113 that σ^{S} would likely constitute a major interacting site of Gp5.7. Therefore, we next
114 focused on identifying the Gp5.7 interacting site on σ^{S}. Nickel affinity pull-down
115 experiments with hexa-histidine tagged σ^{S} (6xHis-σ^{S}) and untagged Gp5.7 were
116 conducted. As shown in Figure 2a, incubation of 6xHis-σ^{S} (lane 2) with whole *E. coli*
117 cell extracts in which untagged Gp5.7 is overexpressed from a plasmid (lane 3) led to
118 the co-purification of untagged Gp5.7 with 6xHis-σ^{S} (lane 5). Control experiments
119 with *E. coli* whole cell extracts with an empty plasmid (Figure 2a, lanes 4 and 6)
120 confirmed that Gp5.7 interacts specifically with 6xHis-σ^{S} and co-purifies with it.
121 Since we showed previously that Gp5.7 interacts with promoter DNA proximal to or
122 overlapping the consensus -35 motif of the T7 A1 promoter, which is also bound by
123 the conserved region 4 (R4) domain of σ factors, we considered whether R4 domain
124 of σ^{S} could be a binding site for Gp5.7. To test this, we conducted affinity pull-down
125 experiments as in Figure 2a using a hexa-histidine tagged version of the R4 domain

126 (amino acid residues 245-330) of σ^S (6xHis-σ^SR4). As shown in Figure 2b (lane 5),
127 we detected untagged Gp5.7 co-purifying with the 6xHis-σ^SR4 domain. In the
128 converse experiment, we repeated affinity pull-down experiments as in Figure 2a
129 using FLAG epitope tagged σ^S lacking the R4 domain (FLAG-$\sigma^S\Delta$R4). As indicated
130 in Figure 2c, and as expected, we failed to detect untagged Gp5.7 co-purifying with
131 the FLAG-$\sigma^S\Delta$R4 protein (lane 5). Based on the affinity pull-down experiments
132 shown in Figure 2a-c, we conclude that the R4 domain of σ^S constitutes the binding
133 site for Gp5.7.
134
135 **Structural insights into the interaction between R4 domain of σ^S and Gp5.7**
136 To independently verify that R4 domain of σ^S constitutes the binding site for Gp5.7
137 within Eσ^S and to map the Gp5.7 interface within R4 of σ^S, we solved the solution
138 structure of the isolated 6xHis-σ^SR4 domain by NMR spectroscopy (Figure 2d and
139 Supplementary Table 1). The structure demonstrates that the R4 domain of σ^S
140 (hereafter referred to as the apo-R4 domain) is able to fold as an isolated subdomain,
141 consisting of five α helices (H1-H5). The α helices H1-H5 superpose well with the
142 equivalent region from the crystal structure of Eσ^S transcription initiation complex, in
143 which the R4 domain (hereafter referred to as the bound-R4 domain) is connected to
144 RNAP subunits via a long and flexible linker [7]. Interestingly, the apo-R4 domain
145 exhibits some conformational differences in the carboxyl (C) and amino (N) termini
146 compared to the bound-R4 domain (Figure 2e). The N-terminus of the apo-R4 domain,
147 which in the bound-R4 domain is connected to Eσ^S via a flexible linker, appears more
148 disordered. The C-terminus of the apo-R4 domain contacts the core of the structure
149 making the apo-R4 domain more compact and stable in the absence of the remaining
150 σ^S domains, RNAP subunits or promoter DNA. We next recorded the 2D ^{1}H-^{15}N

151 HSQC NMR spectra to monitor the backbone amide chemical shift and line-width
152 perturbations for ^{15}N-labelled apo-R4 domain in the presence of up to a 2-fold molar
153 excess of unlabeled Gp5.7. As shown in Figure 2f, several peaks exhibited
154 measurable broadening effects and the extent of broadening correlating with the
155 amount of Gp5.7 added (Figure 2f). The Gp5.7 interaction surface was mapped on the
156 structure of the apo-R4 domain (Figure 2g), revealing that the main interacting
157 residues localise to the C terminal part of H1 and N terminal part of H2. This analysis
158 suggests that Gp5.7 binds between the RNAP facing surface and the promoter-facing
159 surface of R4 of σ^S (notably H3 of 4.2 sub-region of R4; Figure 2d). Overall, the
160 results from the affinity pull-down and structural analyses unambiguously indicate the
161 R4 of σ^S constitutes the binding site for Gp5.7 on σ^S.
162
163 **Gp5.7 inhibits RPo formation by Eσ^S on the T7 A1 promoter**
164 The location of the Gp5.7 binding surface on σ^S implies that Gp5.7 has
165 evolved to target a σ^S domain potentially important for transcription initiation from
166 the T7 A1 promoter. Previous reports from several groups have implied that the
167 interaction between R4 of σ^{70} and the consensus -35 promoter region is required for
168 the stabilization of early intermediate promoter complexes *en route* to the RPo at the
169 T7 A1 promoter [8, 9, 10, 11]. Therefore, we considered whether Gp5.7 inhibits Eσ^S-
170 dependent transcription from the T7 A1 promoter by antagonizing RPo formation. In
171 agreement with this view, whereas Eσ^S reconstituted with $\sigma^S\Delta$R4 was able to initiate
172 transcription from a prototypical Eσ^{70}-dependent promoter i.e. *lac*UV5 (albeit at a
173 lower efficiency compared to reactions with wild-type Eσ^S), we failed to detect any
174 transcription by E$\sigma^S\Delta$R4 from the T7 A1 promoter (Figure 3a). We then conducted
175 electrophoretic gel mobility shift assays at 4°C (to detect initial RNAP-promoter

complex formation) and at 37°C (to detect RPo formation) with Eσ^SΔR4 and a γ-^{32}P-labelled T7 A1 probe to determine whether Eσ^SΔR4 was able to interact with the T7 A1 promoter to form the initial promoter complex or whether the initial promoter complex formed by Eσ^SΔR4 on the T7 A1 promoter was unable to isomerize into the RPo, respectively. Results shown in Figure 3b, demonstrated that although Eσ^S and Eσ^SΔR4 formed the initial promoter complex on the T7 A1 promoter equally well (lanes 2-6), those formed by Eσ^SΔR4 seem unable to isomerize to form the transcriptionally proficient RPo. Consistent with this conclusion, *in vitro* transcription assays with a T7 A1 promoter probe containing an heteroduplex segment between positions -12 and +2 (to mimic the RPo) revealed that Eσ^SΔR4 is able to synthesize the CpApU transcript (Figure 3c, compare lanes 1 and 2 with lanes 3 and 4). In further support of the view that Gp5.7 inhibits RPo formation at the T7 A1 promoter, Eσ^S was able to synthesize the CpApU transcript in the presence of Gp5.7 when the latter was added to a pre-formed RPo (i.e. when Gp5.7 was added to the reaction following pre-incubation of Eσ^S and the homoduplex T7 A1 promoter at 37°C) (Figure 3d). Overall, we conclude that R4 of σ^S is important for RPo formation at the T7 A1 promoter and Gp5.7 inhibits RPo formation by Eσ^S during T7 development by interfering with the R4 of σ^S.

A role for Gp5.7 in managing σ^S during T7 development in stationary phase *E. coli*

The results so far indicate that Eσ^S accumulates as a consequence of (p)ppGpp buildup during T7 development in exponentially growing *E. coli* cells and that Gp5.7 is required to preferentially inhibit Eσ^S activity on T7 A1 promoter. However, when *E. coli* cells are in the stationary phase of growth, the major species of RNAP

201 molecules will contain σ^S (also due to the buildup of (p)ppGpp in response to the
202 stresses encountered by *E. coli* cells in the stationary phase of growth). In addition,
203 (p)ppGpp, together with $E\sigma^S$, also contributes to the shutting-down of cellular
204 activities in the stationary phase of growth. Therefore, the development of a phage
205 can be affected by changes in the growth state, and thus cellular activities, of the
206 bacterial cell. Consistent with this view, Nowicki et al [12] recently reported that
207 progeny production by Shiga toxin converting lamboid phages was significantly more
208 efficient in a *ΔrelA*/*ΔspoT E. coli* (which is unable to synthesize (p)ppGpp) than in its
209 isogenic wild-type strain.

210 A phage plaque is a clearing in a bacterial lawn and plaques form via an
211 outward diffusion of phage progeny virions that prey on surrounding bacteria.
212 Therefore, the rate of plaque-enlargement can serve as a proxy for how efficiently a
213 phage develops and produces progeny within an infected bacterial cell. Further,
214 although the aging of the bacterial lawn often represents a major barrier for plaque-
215 enlargement, T7 plaques have been reported to enlarge continually on matured *E. coli*
216 lawns [13], suggesting that T7 has evolved specific mechanisms to infect and develop in
217 the stationary phase of *E. coli* growth. Therefore, we investigated whether Gp5.7 is
218 required for T7 development in *E. coli* in the stationary phase of growth by measuring
219 plaque size formed on a lawn of *E. coli* as a function of incubation time in the context
220 of a wild-type and *ΔrelA*/*ΔspoT E. coli* strains (recall accumulation of σ^S will be
221 compromised in the mutant strain due to the absence of (p)ppGpp; see above). As
222 shown in Figure 4, the rate of plaque-enlargement and plaque size on a lawn of wild-
223 type *E. coli* infected with T7 wild-type and Δ*gp5.7* phage was indistinguishable for
224 the first 12 hours (Figure 4 and Supplementary Movie 1). However, whereas the wild-
225 type T7 plaques continued to enlarge, the rate at which the plaques formed by T7

226 Δ*gp5.7* enlarged significantly slowed after ~12 hours of incubation and completely
227 ceased after ~20 hours of incubation (Figure 4 and Supplementary Movie 1). Hence,
228 after 72 hours of incubation, the size of the plaque formed by the T7 Δ*gp5.7* phage
229 was ~50% smaller than the plaque formed by the wild-type T7 phage on a lawn of
230 wild-type *E. coli* cells. We were able to partially, yet specifically, revert the rate of
231 plaque-enlargement and plaque size of the T7 Δ*gp5.7* phage to that of the wild-type
232 T7 phage by exogenously providing Gp5.7 from an inducible plasmid in *E. coli*
233 (Supplementary Figure 2).

234 In marked contrast, although the rate of enlargement of the plaques formed by
235 the wild-type T7 phage was similar on a lawn of *ΔrelA*/*ΔspoT E. coli* to that observed
236 on a lawn of wild-type *E. coli* for the first 8 hours of incubation, the plaques formed
237 by the wild-type T7 phage continued to enlarge at a faster rate on a lawn of
238 *ΔrelA*/*ΔspoT E. coli* than on a lawn of wild-type *E. coli* lawn (Figure 4). For example,
239 after 48 hours of incubation, the size of the plaques formed by the T7 wild-type phage
240 on a lawn of *ΔrelA*/*ΔspoT E. coli* was ~2-fold larger than those formed on a lawn of
241 wild-type *E. coli* (Figure 4) Strikingly, whereas the plaques formed by the T7 Δ*gp5.7*
242 phage ceased enlarging after ~20 hours of incubation on a lawn of wild-type *E. coli*,
243 they continued to enlarge (albeit at a slower rate than that of T7 wild-type phage) on a
244 lawn of *ΔrelA*/*ΔspoT E. coli* (Figure 4). Overall, although we cannot fully exclude
245 possibility that the absence of (p)ppGpp in *ΔrelA*/*ΔspoT E. coli* will generally provide
246 a more favorable intracellular conditions for T7 development than in wild-type *E. coli*
247 cells, the results clearly demonstrate that (i) the accumulation of (p)ppGpp during T7
248 infection antagonizes T7 development in *E. coli*; (ii) Gp5.7 represents a mechanism
249 by which T7 overcomes the antagonistic effect of (p)ppGpp-mediated accumulation

250 of σ^S on its development and therefore (iii) Gp5.7 is also a T7 factor required for T7
251 development in *E. coli* cells in the stationary phase of growth.
252
253 **Discussion**
254
255 The inhibition of the host transcription machinery, the RNA polymerase, is a central
256 theme in the strategies used by phages to acquire their bacterial prey. In the
257 prototypical *E. coli* phage T7, the switching from using the host RNAP for
258 transcription of early T7 genes to the T7 RNAP for transcription of middle and late
259 T7 genes is tightly regulated two bacterial RNAP inhibitors: Gp2 and Gp5.7.
260 Dysregulation of this process, for example due to the absence of any of these factors,
261 is believed to lead to steric interference between the host and T7 RNAP molecules on
262 the T7 genome and results in compromised or aborted development of phage progeny
263 [2, 5]. In an earlier study, we proposed that Gp5.7 acts as a 'last line of defense'
264 molecule to prevent aberrant transcription of middle and late T7 genes by host RNAP
265 molecules that have escaped inhibition by Gp2 [5]. The present study has uncovered
266 additional biological roles for Gp5.7 in the T7 development cycle: On one hand, the
267 results show that during infection of exponentially growing *E. coli* cells by T7 phage,
268 Gp5.7 serves to inhibit $E\sigma^S$, which accumulates, possibly as a consequence of the
269 (p)ppGpp-mediated stress response mechanism to T7 infection (Figure 5, box 1-3).
270 On the other hand, Gp5.7 is required for T7 development in *E. coli* in the stationary
271 phase of growth (Figure 5, box 4-6). In the latter case, we envisage that Gp5.7 will be
272 absent when the transcription (of early T7 genes) dependent translocation of the T7
273 genome by $E\sigma^S$ occurs during infection of *E. coli* in the stationary phase of growth
274 (Figure 5, box 4), but becomes available when the $E\sigma^S$ is no longer required, i.e. when

275 the T7 RNAP takes over the transcription of the middle and late genes (Figure 5, box
276 5). The fact that Gp2 only poorly inhibits $E\sigma^{S}$ [4] further supports the need for Gp5.7
277 for T7 development in both exponentially growing and stationary phase *E. coli* cells.
278 Thus, to the best of our knowledge, Gp5.7 is the only phage-encoded host RNAP
279 inhibitor (or phage factor) described to date that is required for successful phage
280 development in stationary phase bacteria. Intriguingly, we are unable to 'rescue' the
281 T7 Δ*gp5.7* phage in a Δ*rpoS E. coli* strain in the context of the plaque-enlargement
282 assay shown in Figure 4. As shown in Supplementary Figure 3, wild-type and Δ*gp5.7*
283 T7 phages are equally compromised to efficiently develop in the Δ*rpoS E. coli* strain.
284 However, since the intracellular levels of $E\sigma^{70}$ will be higher than in the Δ*rpoS E. coli*
285 than in the wild-type *E. coli* due to the absence of the competing σ^{S} [14], we propose
286 that T7 is unable to efficiently develop in the Δ*rpoS E. coli* because of inadequate
287 ability Gp2 and Gp5.7 (and Gp0.7) to inhibit the excess $E\sigma^{70}$ molecules (which will
288 presumably dilute the intracellular pool of Gp2 and Gp5.7 (and Gp0.7) available to
289 fully inhibit $E\sigma^{70}$ to allow optimal T7 development). Overall, our results indicate that,
290 although T7 development in *E. coli* depends on the host RNAP (for transcription-
291 dependent translocation of T7 genome into the bacterial cell and transcription of early
292 T7 genes), efficient management of host RNAP activity is clearly obligatory for T7 to
293 optimally develop both in exponentially-growing and stationary phase *E. coli* cells.
294 Consequently, any perturbations in RNAP levels or activity can have adverse effects
295 on T7 development.

296 We further note that, although Gp2 and Gp5.7 bind to sites located at different
297 faces of the RNAP (with respect to the active center of the RNAP, the Gp2 binding
298 site is located on the β' jaw domain at the downstream face of the RNAP [15], whereas
299 Gp5.7 binding site is located at the upstream face of the RNAP (this study)), both T7

300 proteins seem to inhibit RPo formation by misappropriation of essential domains of
301 the σ factor (region 1 of σ^{70} in case of Gp2 [4 16] and R4 of σ^{S} in the case of Gp5.7 (this
302 study)). Since the R4 domain of σ^{70} is also targeted by a T4 phage protein, called
303 AsiA, to 'recruit' the host RNAP to transcribe phage genes (reviewed in [17]), it is
304 interesting to speculate whether phages, regardless of their dependence on the host
305 RNAP (unlike T7 phage, the T4 phage fully relies on the host RNAP for the
306 transcription of its genes), have evolved a common mechanism to misappropriate
307 essential bacterial σ factors domains to inhibit (e.g. T7) or redirect (e.g. T4) host
308 RNAP activity to serve phage developmental requirements.

309 In summary, our study has uncovered a new aspect of T7 biology and the
310 distinct strategies used by this phage to shut down bacterial RNAP for an optimal
311 infection outcome in *E. coli* in exponentially growing and stationary phases of
312 growth. The latter is clearly relevant to bacteria encountered by T7 in the natural
313 environment, which are often in a starved and thus in a growth-attenuated or slow
314 growing state. Therefore, the insights from this study also have implications on the
315 emerging interest in the use of phages, phage-derived antibacterial compounds and
316 their bacterial targets to treat bacterial infections where bacteria largely exist in a
317 'stressed' state and mostly depend on $E\sigma^{S}$ dependent gene expression for survival [18].

318

319 **Methods**

320 **(p)ppGpp measurements.** A culture of *E. coli* MG1655 *rpoC*-FLAG was setup from
321 an overnight culture in 5 ml potassium morpholinopropane sulfonate (MOPS)
322 minimal media with a starting OD_{600} of 0.05 at 37°C. At OD_{600} 0.1, 20 μCi/ml [^{32}P]
323 H_3PO_4 was added as phosphate source and culture was left to grow to an OD_{600} of
324 0.45. The culture was then infected with T7 WT (ratio of 10:1 – T7:*E. coli*) in the

325 presence of 1 mM $CaCl_2$. To detect (p)ppGpp production, 500 µl of the cultures prior
326 to infection (time 0) and at 10 min after infection were added to 100 µl of ice cold 2
327 M formic acid and incubated on ice for 30 min. The samples were then centrifuged
328 for 5 min at 17,000*g* and 10 µl of supernatant were spotted on thin layer
329 chromatography (TLC) polyethylenimine (PEI) cellulose F (dimensions 20 cm x 20
330 cm [Merck Millipore]). The spot was left to migrate to the top of the sheet in a TLC
331 tank in presence of 1.5 M KH_2PO_4 pH 3.6, dried before exposing overnight onto
332 phosphor screen and viewed using Phosphoimager. For a positive control, 100 µg/ml
333 serine hyroxamate (SHX) was added to MG1655 *rpoC*-FLAG at OD_{600} of 0.45 and
334 sample taken and processed as above.
335
336 **Western blotting.** *E. coli* MG1655 *rpoC*-FLAG strain was grown in LB at 30°C to an
337 OD_{600} of ~0.45. The culture was then infected with T7 WT (ratio of 0.1:1 – T7:*E.*
338 *coli*) in the presence of 1 mM $CaCl_2$. To detect σ^S production, 20 ml of the culture
339 prior to infection (time 0) and at 10 min intervals after infection were taken until
340 complete lysis was obtained. Experiments with the MG1655 Δ*relA*/Δ*spoT* strain ([19];
341 kindly provided by Kenn Gerdes) were conducted exactly as described above but
342 samples were taken at 0 and 40 min after T7 infection. Cultures were centrifuged, cell
343 pellets re-suspended in 500 µl of 20 mM Na_2PO_4, 50 mM NaCl and 5% glycerol and
344 sonicated. The cleared cell lysate was then loaded on 4-20% SDS-PAGE and ran at
345 200 V for 30 min. The SDS-PAGE gel was transferred onto polyvinylidene difluoride
346 (PVDF) membrane (0.2 µm) using Trans-Blot® Turbo™ Transfer System [Bio-Rad]
347 device and processed according to standard molecular biology protocols. The primary
348 antibodies were used at the following titres: anti-*E. coli* RNAP σ^S antibody at 1:500
349 [1RS1 – Biolegend], anti-*E. coli* RNAP α-subunit antibody at 1:1000 [4AR2 –

350 Biolegend]. The secondary antibody Rabbit Anti-Mouse IgG H&L (HRP) was used at
351 1:2500 [ab97046—Abcam]. Bands were detected using an Amersham ECL Western
352 Blotting Detection Reagent [GE Healthcare Life Sciences] and analysed on a
353 Chemidoc using the Image Lab Software.
354
355 **Protein expression and purification.** FLAG-tagged *E. coli* σ^{70} and σ^{S} were PCR
356 amplified from *E. coli* genome and cloned into the pT7-FLAG™-1 vector [Sigma-
357 Aldrich]. Recombinant vectors pT7-FLAG::*rpoD* and pT7-FLAG::*rpoS* were
358 confirmed by DNA sequencing. For the biochemical experiments, recombinant
359 FLAG-tagged *E. coli* σ^{70} and σ^{S} were made by FLAG affinity purification from *E. coli*
360 strain BL21 (DE3). Briefly, the culture of BL21 (DE3) cells containing pT7-
361 FLAG::*rpoD* was grown at 37°C to an OD_{600} of ~0.4, cold shocked on ice for 15 min
362 before protein expression was induced with 0.1 mM IPTG. The cells were left to grow
363 at 16°C overnight before harvesting. For FLAG-tagged *E. coli* σ^{S} expression, BL21
364 (DE3) containing pT7-FLAG::*rpoS* were grown at 37°C to an OD_{600} of ~0.4 and
365 protein expression was induced with 0.1 mM IPTG. The cells were left to continue
366 growing at 37°C for 3 h before harvesting. The cell pellet for both FLAG-tagged *E.*
367 *coli* σ^{70} and σ^{S} were re-suspended in binding buffer (50 mM Tris-HCl, 150 mM NaCl,
368 pH 7.4) containing cocktail of protease inhibitors and lysed by sonication. The cleared
369 cell lysate was loaded to a column containing anti-FLAG M2 affinity gel [Sigma-
370 Aldrich] and the purified proteins were obtained by adding elution buffer (100 μg/ml
371 3XFLAG® peptide [Sigma-Aldrich] in binding buffer) for 30 min at 4°C. The purified
372 proteins were dialyzed into storage buffer (10 mM Tris-HCl pH 8.0, 50 mM NaCl,
373 50% glycerol, 0.1 mM EDTA and 1 mM DTT) and stored in aliquots at -80°C. The
374 FLAG-tagged $\sigma^{S}\Delta$R4 (amino acid residues 1-262) was made by introducing a stop

375 codon into pT7-FLAG::*rpoS* by site-directed mutagenesis and its expression and
376 purification was done as described for the full-length protein. The 6xHis-σ^SR4 (amino
377 acid residues 245-330) was amplified from *E. coli* genomic DNA by Gibson assembly
378 and ligated into the pET-46 Ek/LIC vector [Merck Millipore] and expressed in *E. coli*
379 strain BL21 (DE3) for the pull-down experiments and structural studies. The cells
380 were grown in either LB (for pull-down experiments) or M9 Minimal medium
381 labelled with ^{15}N and ^{13}C (for the structural studies) and induced with 0.5 mM IPTG
382 when the OD_{600} reached 0.6 and incubated overnight at 18°C before harvesting by
383 centrifugation. The cells were lysed by sonication in 50 mM NaH_2PO_4, 300 mM
384 NaCl, 10 mM imidazole pH 8 and purified using Ni-NTA beads [Qiagen]. The eluate
385 was then dialyzed against 50 mM NaH_2PO_4 and 350 mM NaCl, at pH 6 and
386 subsequently concentrated down for NMR experiments whilst for pull-down
387 experiments, the 6xHis-σ^SR4 protein was kept in 50 mM NaH_2PO_4, 300 mM NaCl,
388 and 10 mM imidazole pH 8. The 6xHis-σ^S was amplified from *E. coli* genomic DNA,
389 cloned into pET-46 Ek/LIC vector [Merck Millipore] by Gibson assembly, expressed
390 and purified as described for 6xHis-σ^SR4. The cells were lysed by sonication under
391 denaturing condition containing 8M urea, purified with Ni-NTA beads under
392 denaturing conditions and the denatured 6xHis-σ^s was refolded in 50 mM NaH_2PO_4,
393 300 mM NaCl, and 10 mM imidazole pH 8. The 6xHis-Gp5.7 was amplified from
394 pBAD18::*gp5.7* [5] and cloned into pET-46 plasmid. The Histidine tag on Gp5.7 was
395 deleted to express tag-free Gp5.7 using Q5 site directed mutagenesis kit [NEB]. The
396 protein was expressed under the same condition as 6xHis-σ^SR4. Recombinant 6xHis-
397 Gp5.7 and 6xHis-Gp2 expression and purification were done exactly as previously
398 described [15]. Sequences of all oligonucleotides used in the construction of the
399 expression vectors are available upon request.

400

401 ***In vitro* transcription assays.** These were conducted exactly as previously described
402 [5] in 10 mM Tris pH 7.9, 40 mM KCl, 10 mM $MgCl_2$ using *E. coli* core RNAP from
403 NEB and FLAG-tagged versions of σ^{70} and σ^S were purified exactly as described
404 above. Reactions in Figures 3c and 3d were conducted in 100 mM K-glutamate, 40
405 mM HEPES pH 8, 10 mM $MgCl_2$ and 100 µg/ml BSA. In all reactions Gp5.7 or Gp2
406 was pre-incubated with $E\sigma^S$ or $E\sigma^{70}$ at the indicated concentrations before adding
407 promoter DNA to the reaction. In the reactions shown in Figure 3d, Gp5.7 was added
408 to the pre-formed RPo (i.e. following pre-incubation of $E\sigma^S$ and the promoter DNA).
409 Sequences of all oligonucleotides used to generate promoter probes are available in [5]
410 or upon request.

411

412 **Pull-down assays**. For the pull-down assays shown in Figure 2a and 2b, Ni-NTA
413 beads [Qiagen] were used. Approximately 0.02 mg of recombinant 6xHis-σ^S or
414 6xHis-σ^SR4 in binding buffer (50 mM NaH_2PO_4, 300 mM NaCl, and 10 mM
415 imidazole pH 8) was added to beads and incubated at 4°C for 30 min. *E. coli* whole-
416 cell lysate containing overexpressed untagged Gp5.7 was added to resin containing
417 sigma and incubated for 1 h at 4°C. The beads were washed three times in 1 ml wash
418 buffer (50 mM NaH_2PO_4, 300 mM NaCl, and 20 mM imidazole pH 8) for 10 min to
419 remove any non-specific protein–protein interaction. To elute samples from beads,
420 elution buffer containing 250 mM imidazole was added. For FLAG-tag protein pull-
421 down assay (Figure 2c), 0.02 mg FLAG-$\sigma^S\Delta$R4 was incubated with anti-FLAG M2
422 affinity gel [Sigma-Aldrich] in 50 mM Tris HCl, pH 7.4, 150 mM NaCl, 1 mM EDTA
423 at 4°C for 2 h. *E. coli* whole-cell lysate containing overexpressed untagged Gp5.7 was
424 added to resin containing sigma and incubated for 2 h at 4°C. The beads were washed

425 three times in 50 mM Tris HCl, pH 7.4, 150 mM NaCl, 1 mM EDTA and 1% Triton
426 X-100 for 10 min to remove any non-specific protein–protein interaction. To elute
427 samples from beads, elution buffer containing 100 µg/ml 3XFLAG® peptide [Sigma-
428 Aldrich] was added. Ten microliters of samples together with Laemmli 2x concentrate
429 SDS Sample Buffer was loaded on a 10–15% SDS-PAGE alongside Protein standard
430 Marker and stained Coomassie Brilliant Blue.

431

432 **NMR structure determination.** NMR spectra were collected at 310K on Bruker
433 DRX600 and DRX800 spectrometers equipped with cryo-probes. Spectral
434 assignments were completed using our in-house, semi-automated assignment
435 algorithms and standard triple-resonance assignment methodology [20]. H_α and H_β
436 assignments were obtained using HBHA (CBCACO)NH and the full side-chain
437 assignments were extended using HCCH-total correlation (TOCSY) spectroscopy and
438 (H)CC(CO)NH TOCSY. Three-dimensional ^{1}H-^{15}N/^{13}C NOESY-HSQC (mixing time
439 100 ms at 800 MHz) experiments provided the distance restraints used in the final
440 structure calculation [21]. The ARIA protocol was used for completion of the NOE
441 assignment and structure calculation. The frequency window tolerance for assigning
442 NOEs was ±0.025 ppm and ±0.03 ppm for direct and indirect proton dimensions and
443 ±0.6 ppm for both nitrogen and carbon dimensions. The ARIA parameters p, Tv and
444 Nv were set to default values. 108 dihedral angle restraints derived from TALOS+
445 were also implemented. The 10 lowest energy structures had no NOE violations
446 greater than 0.5 Å and dihedral angle violations greater than 5°. The structural
447 statistics are shown in Supplementary Table 1.

448

449 **NMR titration.** Unlabeled Gp5.7 was added to ^{15}N labelled 6xHis-σ^SR4 according to
450 stoichiometric ratio to perform NMR titration. Maximum five-fold Gp5.7 was added
451 to 6xHisσ^SR4 in order to broad out the entire spectra.

452

453 **Electrophoretic mobility shift assays.** These were conducted exactly as previously
454 described to distinguish between initial promoter complex and RP_O formation [15].
455 Briefly, 75 nM of *E. coli* core RNAP (NEB) was incubated with 300 nM σ^S or $\sigma^S\Delta$R4
456 either on ice (to monitor initial promoter complex formation) or at 37°C (to monitor
457 RP_O formation) for 5 min in 100 mM K-glutamate, 40 mM HEPES pH 8, 10 mM
458 $MgCl_2$ and 100 µg/ml BSA. Twenty nanomolar of ^{32}P-labelled T7 A1p was added and
459 incubated for 5 min. Since initial promoter complexes (formed at temperatures < 4
460 °C) are sensitive to heparin and, conversely, RP_O are resistant to heparin, the reactions
461 were challenged with 100 µg/ml heparin before separating the RNAP bound and free
462 promoter DNA by native gel electrophoresis on a 4.5% (w/v) native polyacrylamide
463 gel run at 100 V for 100 min at 4°C (to monitor initial promoter complex formation)
464 or 60 min at room temperature (to monitor RP_O formation). The dried gel was then
465 analyzed by autoradiography.

466

467 **Plaque-enlargement assay.** T7 phage plaques were formed as described in [5]. To
468 obtain images of plaques, *E. coli* MG1655 cultures and MG1655 Δ*relA*/Δ*spoT* were
469 grown to an OD_{600} of 0.45 in LB at 30°C and 300 µl aliquots of the culture were taken
470 out and either T7 wild-type or T7 Δ*gp5.7* lysate (sufficient to produce ~ 10 plaques)
471 were added together with 1 mM $CaCl_2$ and incubated at 37°C for 10 min to allow the
472 phage to adsorb to bacteria. Three milliliters of 0.7% (w/v) top agar was added to
473 each sample and plated onto plates containing exactly 20 ml of 1.5% (w/v) LB agar.

474 The plates were then put in a Epson perfection V370 photo scanner [Model J232D]
475 inside a 30°C incubator and images of the plates were taken every two hours over a
476 72 h period for analysis. For complementation experiments, *E. coli* MG1655 cells
477 containing either pBAD18::empty or pBAD18::*gp5.7* or pBAD18::*gp5.7-L42A* [5] were
478 used and the plaque-enlargement assay was carried out as above on plates containing
479 100 μg/ml ampicillin and 0.04% (w/v) L-arabinose to induce *gp5.7* expression. The
480 MG1655 Δ*rpoS* strain was obtained by phage transduction from *ΔrpoS* mutant in
481 Keio libray [22].
482

483 **References**

484 1. Kemp P, Gupta M, Molineux IJ. Bacteriophage T7 DNA ejection into cells is
485 initiated by an enzyme-like mechanism. *Mol Microbiol* **53**, 1251-1265
486 (2004).
487
488 2. Savalia D, Robins W, Nechaev S, Molineux I, Severinov K. The role of the
489 T7 Gp2 inhibitor of host RNA polymerase in phage development. *J Mol*
490 *Biol* **402**, 118-126 (2010).
491
492 3. Severinova E, Severinov K. Localization of the Escherichia coli RNA
493 polymerase beta' subunit residue phosphorylated by bacteriophage T7
494 kinase Gp0.7. *J Bacteriol* **188**, 3470-3476 (2006).
495
496 4. James E*, et al.* Structural and mechanistic basis for the inhibition of
497 Escherichia coli RNA polymerase by T7 Gp2. *Mol Cell* **47**, 755-766 (2012).
498
499 5. Tabib-Salazar A*, et al.* Full shut-off of Escherichia coli RNA-polymerase by
500 T7 phage requires a small phage-encoded DNA-binding protein. *Nucleic*
501 *Acids Res* **45**, 7697-7707 (2017).
502
503 6. Friesen JD, Fiil N. Accumulation of guanosine tetraphosphate in T7
504 bacteriophage-infected Escherichia coli. *J Bacteriol* **113**, 697-703 (1973).
505
506 7. Liu B, Zuo Y, Steitz TA. Structures of E. coli sigmaS-transcription initiation
507 complexes provide new insights into polymerase mechanism. *Proc Natl*
508 *Acad Sci U S A* **113**, 4051-4056 (2016).
509
510 8. Chen H, Tang H, Ebright RH. Functional interaction between RNA
511 polymerase alpha subunit C-terminal domain and sigma70 in UP-

512 element- and activator-dependent transcription. *Mol Cell* **11**, 1621-1633
513 (2003).
514
515 9. Ross W, Schneider DA, Paul BJ, Mertens A, Gourse RL. An intersubunit
516 contact stimulating transcription initiation by E coli RNA polymerase:
517 interaction of the alpha C-terminal domain and sigma region 4. *Genes Dev*
518 **17**, 1293-1307 (2003).
519
520 10. Minakhin L, Severinov K. On the role of the Escherichia coli RNA
521 polymerase sigma 70 region 4.2 and alpha-subunit C-terminal domains in
522 promoter complex formation on the extended -10 galP1 promoter. *J Biol*
523 *Chem* **278**, 29710-29718 (2003).
524
525 11. Sclavi B, Zaychikov E, Rogozina A, Walther F, Buckle M, Heumann H. Real-
526 time characterization of intermediates in the pathway to open complex
527 formation by Escherichia coli RNA polymerase at the T7A1 promoter.
528 *Proc Natl Acad Sci U S A* **102**, 4706-4711 (2005).
529
530 12. Nowicki D, Kobiela W, Wegrzyn A, Wegrzyn G, Szalewska-Palasz A.
531 ppGpp-dependent negative control of DNA replication of Shiga toxin-
532 converting bacteriophages in Escherichia coli. *J Bacteriol* **195**, 5007-5015
533 (2013).
534
535 13. Yin J. Evolution of bacteriophage T7 in a growing plaque. *J Bacteriol* **175**,
536 1272-1277 (1993).
537
538 14. Farewell A, Kvint K, Nystrom T. Negative regulation by RpoS: a case of
539 sigma factor competition. *Mol Microbiol* **29**, 1039-1051 (1998).
540
541 15. Camara B*, et al.* T7 phage protein Gp2 inhibits the Escherichia coli RNA
542 polymerase by antagonizing stable DNA strand separation near the
543 transcription start site. *Proc Natl Acad Sci U S A* **107**, 2247-2252 (2010).
544
545 16. Bae B, Davis E, Brown D, Campbell EA, Wigneshweraraj S, Darst SA. Phage
546 T7 Gp2 inhibition of Escherichia coli RNA polymerase involves
547 misappropriation of sigma70 domain 1.1. *Proc Natl Acad Sci U S A* **110**,
548 19772-19777 (2013).
549
550 17. Hinton DM. Transcriptional control in the prereplicative phase of T4
551 development. *Virol J* **7**, 289 (2010).
552
553 18. Dong T, Schellhorn HE. Role of RpoS in virulence of pathogens. *Infect*
554 *Immun* **78**, 887-897 (2010).
555
556 19. Magnusson LU, Gummesson B, Joksimovic P, Farewell A, Nystrom T.
557 Identical, independent, and opposing roles of ppGpp and DksA in
558 Escherichia coli. *J Bacteriol* **189**, 5193-5202 (2007).
559

20. Marchant J, Sawmynaden K, Saouros S, Simpson P, Matthews S. Complete resonance assignment of the first and second apple domains of MIC4 from Toxoplasma gondii, using a new NMRView-based assignment aid. *Biomol NMR Assign* **2**, 119-121 (2008).

21. Pardi A. Multidimensional heteronuclear NMR experiments for structure determination of isotopically labeled RNA. *Methods Enzymol* **261**, 350-380 (1995).

22. Baba T, *et al.* Construction of Escherichia coli K-12 in-frame, single-gene knockout mutants: the Keio collection. *Mol Syst Biol* **2**, 2006 0008 (2006).

Acknowledgements

We would like to thank Daniel Brown for help with the (p)ppGpp measurements. This work was supported by Wellcome Trust awards to SM (Investigator Award 100280 and multiuser equipment grant 104833) and SW (Investigator Award 100958).

Author contributions

A.T-S., B.L., S.W. and S.M. designed research; A.T-S., B.L., L.B., and D.B. preformed research; S.W., S.M., A.T-S., B.L., and U.Q. analyzed data and S.W., S.M., A.T-S and B.L. wrote the paper.

[a]A.T-S and B.L. contributed equally to this work.

Figure legends

Figure 1. Gp5.7 is an inhibitor of the *E. coli* stationary phase RNAP, Eσ^S. (a) PEI cellulose showing (p)ppGpp production during T7 infection. Lane 1: before T7 infection, lane 2: 10 min after infection with T7 and lane 3: positive control showing (p)ppGpp production in response to addition of sodium hydroxamate (SHX). The migration positions of ppGpp and (p)ppGpp and the origin where the samples were

591 spotted are indicated. **(b)** Expression of σ^S during T7 infection. *Top*: Graph showing
592 the optical density (OD_{600nm}) of wild-type and Δ*relA*/Δ*spoT E. coli* cultures as a
593 function of time after infection with T7 phage. *Bottom*: Image of a Western blot
594 probed with anti-σ^S and anti-RNAP α-subunit (loading control) antibodies. Lanes 1 to
595 5 contain whole cell extracts of wild-type *E. coli* cells at 0, 10, 20, 30 and 40 min
596 after infection with T7; lanes 6 and 7 contain whole cell extracts of Δ*relA*/Δ*spoT E.*
597 *coli* cells at 0 and 40 min after infection with T7. **(c)** Autoradiograph of denaturing
598 gels comparing the ability of the $E\sigma^S$ and $E\sigma^{70}$ to synthesize a dinucleotide-primed
599 RNA product from the T7 A1 promoter in the absence and presence of Gp2 and
600 Gp5.7. The dinucleotide used in the assay is underlined and the asterisks indicate the
601 radiolabeled nucleotide. The concentration of $E\sigma^S$ and $E\sigma^{70}$ was 75 nM and Gp2 and
602 Gp5.7 were present at 75, 150 and 300 and 1200, 1500 and 1875 nM, respectively.
603 The percentage of RNA transcript synthesized (%A) in the reactions containing Gp5.7
604 or Gp2 with respect to reactions with no Gp5.7 or Gp2 added is given at the bottom of
605 the gel and the value obtained in at least three independent experiments fell within 3–
606 5% of the %A value shown.
607
608 **Figure 2. Structural insights into the interaction between R4 domain of σ^S and**
609 **Gp5.7. (a)** Image of a denaturing gel showing that 6xHis-σ^S pulls down
610 overexpressed untagged Gp5.7 from *E. coli* whole cell lysate. The migration positions
611 of the Gp5.7 and 6xHis-σ^S are indicated. **(b)** As in (a), but using 6xHis-σ^SR4 domain.
612 **(c)** As in (a), but using FLAG-σ^SΔR4. **(d)** *Left*: Cartoon representation of apo-σ^SR4
613 solution structure. *Right:* The image on the left rotated 180° clockwise with the α-
614 helices corresponding to R4 sub-regions 4.1 (in green) and 4.2 (in blue) indicated. **(e)**
615 Overlay of cartoon representations of apo-σ^SR4 domain (orange) and bound-σ^SR4

616 domain (cyan). **(f)** Overlay of 2D ^{1}H-^{15}N HSQC spectra of the apo-σ^{S}R4 without
617 (black) and with Gp5.7 (red) recorded at pH 6.0, 300 K. Peaks that experienced
618 broadening or chemical shift perturbation are labelled according to the amino acid
619 residues in σ^{S}. **(g)** A surface representation of apo-σ^{S}R4 showing the regions
620 interfacing with Gp5.7 (amino acid residues with significant peak broadening and
621 chemical shift perturbation are shown in red, while those that experience moderate
622 peak broadening and chemical shift perturbation are shown in orange and those that
623 experience weak peak broadening and chemical shift perturbation are shown in
624 yellow); amino acid residues associated with interacting with or proximal to the
625 promoter DNA (raspberry) and RNAP subunits (grey) are also shown.
626
627 **Figure 3. Gp5.7 inhibits RP**o **formation by Eσ^{S} on the T7 A1 promoter. (a)**
628 Autoradiograph of denaturing gels showing the ability of the Eσ^{S}ΔR4 to synthesize a
629 dinucleotide-primed RNA product from the T7 A1 and *lac*UV5 promoters. The
630 dinucleotide used in the assay is underlined and the asterisks indicate the radiolabeled
631 nucleotide. **(b)** Autoradiographs of non-denaturing gels showing the ability of Eσ^{S}
632 and Eσ^{S}ΔR4 to form the initial promoter complex and the RP_{O} on the T7 A1
633 promoter. The migration positions of promoter complexes and free DNA are
634 indicated. Reactions to which heparin were added are indicated. See methods for
635 details. **(c)** As in (a) but using the T7 A1 homoduplex and heteroduplex (-12 to +2)
636 promoters. **(d)** As in (a) but Gp5.7 (1875 nM) was added to the pre-formed RPo
637 (formed using 75 nM Eσ^{S} (see text for details).
638
639 **Figure 4. A role for Gp5.7 in managing σ^{S} during T7 development in stationary**
640 **phase *E. coli.*** *Top:* Representative scanned images of T7 wild-type and T7 Δ*gp5.7*

641 plaques formed on a lawn of wild-type *E. coli* and Δ*relA*/Δ*spoT E. coli* over a 72 h
642 incubation period. *Bottom:* Graph showing plaque size (%P) as percentage (%P) of
643 final plaque size formed by wild-type T7 phage on a lawn of wild-type *E. coli* after 72
644 h of incubation (set at 100%) as a function of incubation time.
645
646 **Figure 5. Model describing the distinct mechanisms which host inhibit host**
647 **RNAP during T7 development in exponentially growing and stationary phase *E.***
648 ***coli* cells.**
649
650
651
652
653
654
655
656
657
658
659
660
661
662
663
664
665

666 **Figure 1.**

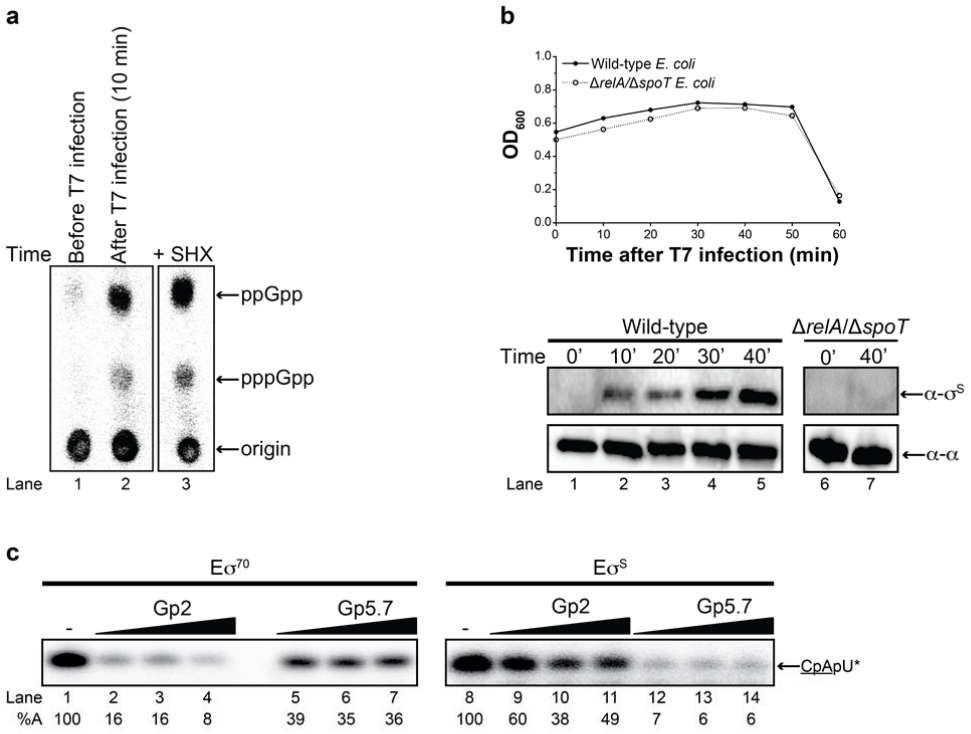

667

668

669

670

671

672

673 **Figure 2.**

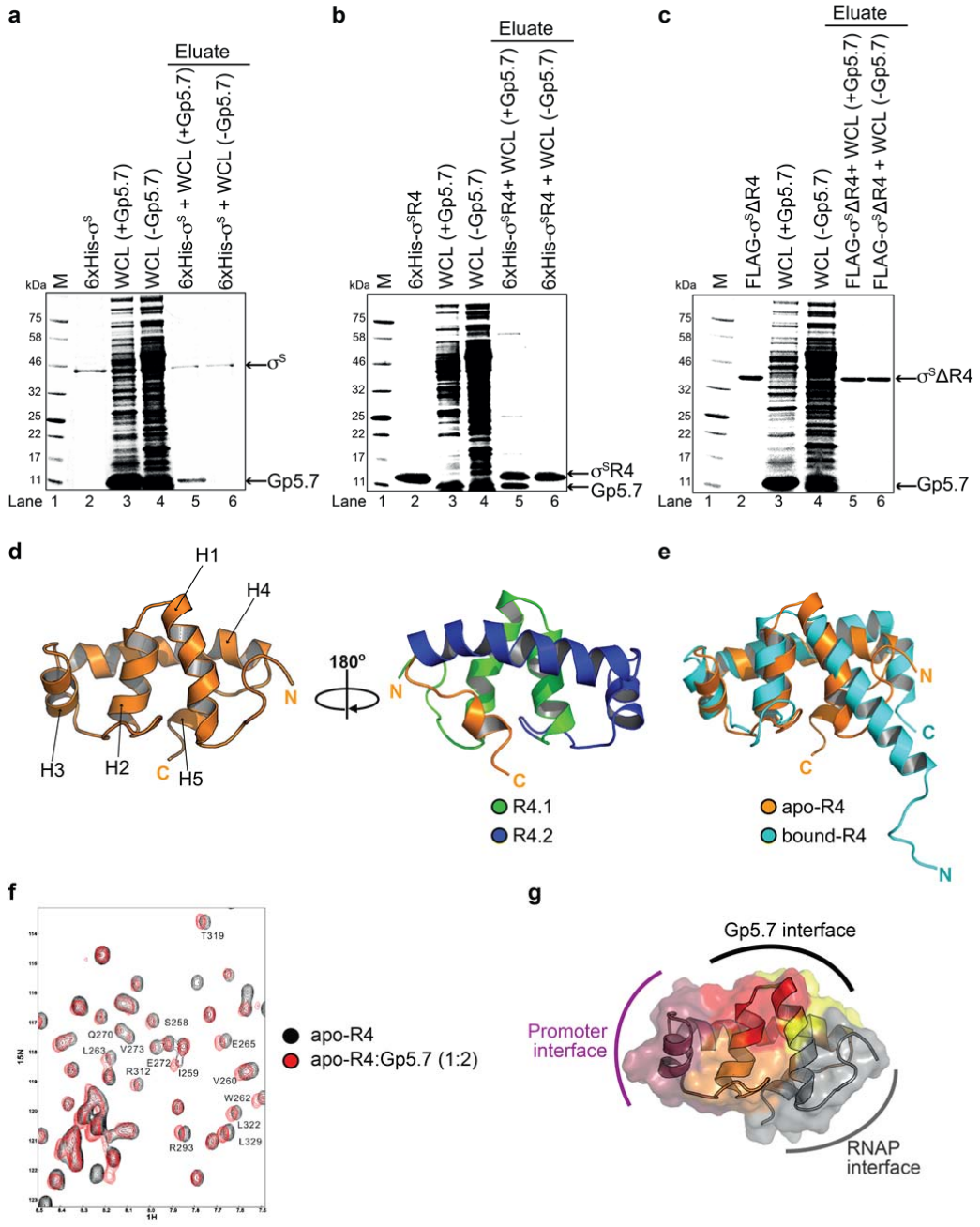

674

675

676

677

678

679

680 **Figure 3.**

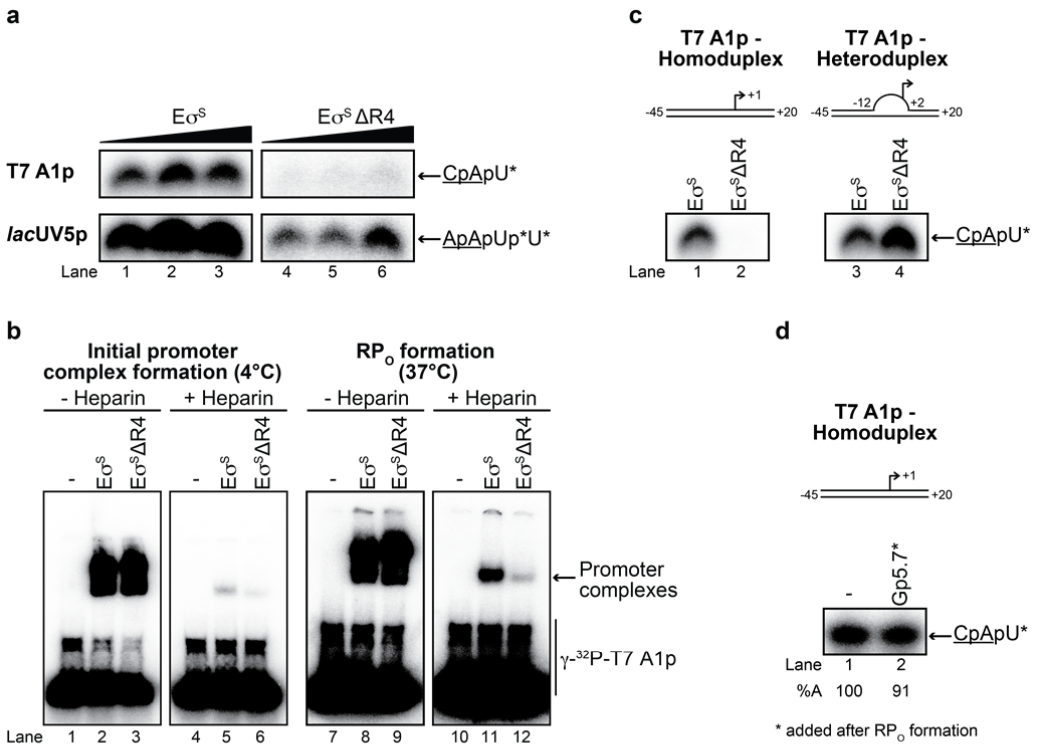

681

682

683

684

685

686

687 **Figure 4.**

688

689

690

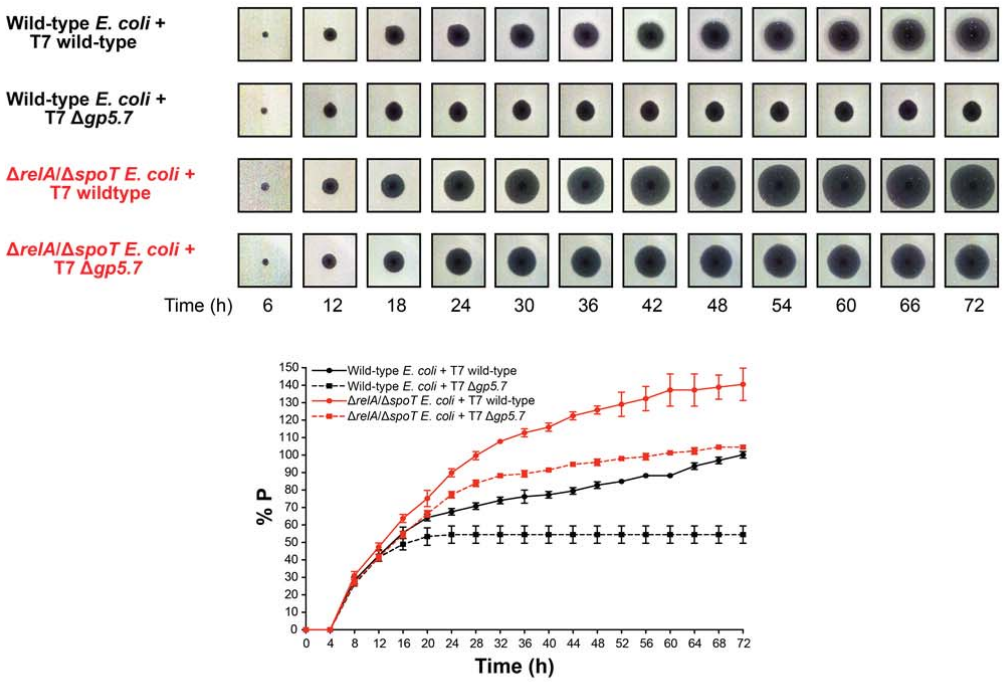

691

692

693

694 **Figure 5.**

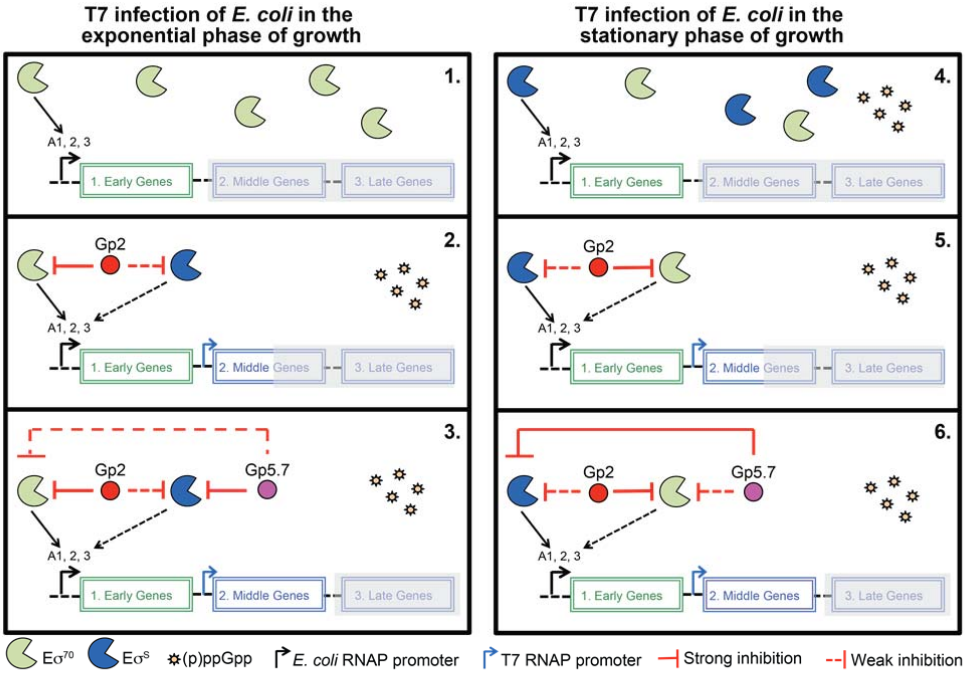

695

Supplementary Information

Supplementary Figure legends

Supplementary Figure 1. Autoradiograph of denaturing gels showing the ability of ability of $E\sigma^S$ to synthesize a dinucleotide-primed RNA product from the T7 A1 promoters in the absence and presence of either wild-type Gp5.7 or Gp5.7-L42A mutant. The dinucleotide used in the assay is underlined and the asterisks indicate the radiolabeled nucleotide. The concentration of $E\sigma^S$ was 75 nM and Gp5.7/Gp5.7-L42A was present at 1200, 1500 and 1875 nM. The percentage of RNA transcript synthesized (%A) in the reactions containing Gp5.7 or Gp5.7-L42A with respect to reactions with no Gp5.7 or Gp5.7-L42A added is given at the bottom of the gel and the value obtained in at least three independent experiments fell within 3–5% of the %A value shown.

Supplementary Figure 2. Graph showing plaque size (%P) of wild-type and Δ*gp5.7* T7 phage on lawns of different *E. coli* cells (as indicated) as percentage of final plaque size of wild-type T7 phage on a lawn of wild-type *E. coli* (containing pBAD18::empty) at 72 h (set at 100%) as a function of time over a 72 h incubation period. The bacterial lawns were grown on agar plates containing L-arabinose to induce Gp5.7 expression. The pBAD18::*gp5.7-L42A* plasmid expressed a functionally-deleterious mutant variant of Gp5.7 (see text for details).

Supplementary Figure 3. Graph showing plaque size (%P) of wild-type and Δ*gp5.7* T7 phage on lawns of different *E. coli* cells (as indicated) as percentage of final plaque size of wild-type T7 phage on a lawn of wild-type *E. coli* at 72 h (set at 100%) as a function of incubation time.

Supplementary Movie 1. Time-lapse movie of plaque formation by T7 wild-type phage (*left*) and T7 Δ*gp5.7* phage (right) on lawns of wild-type *E. coli* over 72 h incubation period.

Supplementary Table

Supplementary Table 1. Structural statistics from the solution structure calculation for 6xHis-σ^SR4 (PDB ID: 6FI7, BMRB ID 34234).

NMR Distance and Dihedral Constraints	
Distance constraints	
Total NOE	1747
Intraresidue	652
Interresidue	1095
Sequential (|*i-j*|)=1)	414
Short range (2≤|*i-j*|)≤3)	278
Medium range (4≤|*i-j*|)≤5)	136
Long range (|*i-j*|)>5)	267
Total Dihedral angle Restraints	108
Φ	76
Ψ	76
Total RDCs	0
Structural Statistics	
Violations (mean and SD)	
Distance constraints (Å)	0.0209 ± 0.0027
Dihedral angle constraints (°)	0.41 ± 0.073
Maximum dihedral angle violation (°)	0.82
Maximum distance constraint violation (Å)	0.23
Deviations from idealized geometry	
Bond length (Å)	0.0038 ± 0.000
Bond angle (°)	0.55 ± 0.012
Impropers (°)	1.44 ± 0.11
Average Pairwise rmsd$^{\alpha}$(Å)	
Heavy	0.679 ± 0.0606
Backbone	0.396 ± 0.0947

Supplementary Figures

Supplementary Figure 1.

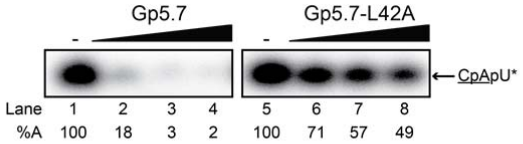

52 **Supplementary Figure 2.**
53

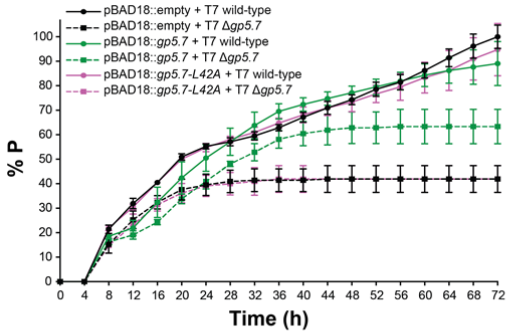

54
55
56
57
58
59
60
61
62
63
64
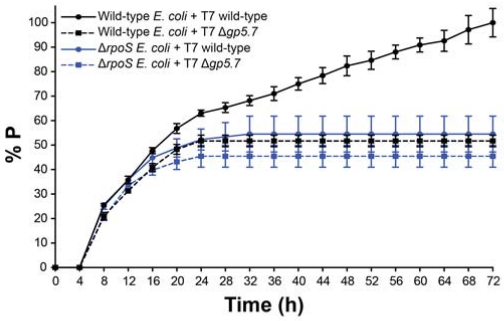
Supplementary Figure 3.